RSC Sustainability

ROYAL SOCIETY OF CHEMISTRY

PAPER

View Article Online
View Journal | View Issue

Cite this: *RSC Sustainability*, 2025, **3**, 1507

Activated carbon derived from rice husks enhanced by methylene blue and gamma irradiation for supercapacitor applications†

Thannithi Anusonthiwong,‡[a] Natavoranun Suwatanapongched,‡[a] Jittiyada Surawattanawiset,‡[a] Nattamon Chittreisin,[b] Somlak Ittisanronnachai,[b] Tanagorn Sangtawesin *[c] and Suranan Anantachaisilp *[a]

Received 11th November 2024
Accepted 23rd January 2025

DOI: 10.1039/d4su00701h

rsc.li/rscsus

Electrodes for supercapacitors were developed from activated carbon (GAC) derived from glutinous rice husk (GRH). The production of GAC involved the chemical activation of GRH with potassium hydroxide (KOH), followed by carbonization at 800 °C for 2 hours under a N_2 atmosphere. The pseudocapacitive effects of the GAC were enhanced through N/S doping by adsorption of methylene blue, followed by post-treatment. Two post-treatment methods were employed in this study: gamma irradiation at doses of 25 kGy (GAC-25), 50 kGy (GAC-50), and 100 kGy (GAC-100), and hydrothermal treatment (GAC-Hdt). Among all samples, GAC-25 exhibited the highest specific capacitance of 127.9 F g^{-1} at 0.5 A g^{-1}, an 84.8% enhancement compared to GAC alone, attributed to pseudocapacitive effects. GAC-25 shows pseudocapacitor behavior, while GAC-Hdt shows EDLC characteristics at an increased scan rate. GAC-Hdt possessed a specific capacitance value of 0.5 A g^{-1}, about four-fold higher than that of GAC-25, due to its larger specific surface area of 1846 m^2 g^{-1}. These results highlight the potential use of gamma irradiation as an alternative post-treatment method for developing supercapacitor electrodes.

Sustainability spotlight

This research contributes to SDG 7 (Affordable and Clean Energy) and SDG 12 (Responsible Consumption and Production) by developing sustainable supercapacitor electrodes from rice husk, an agricultural by-product. Utilizing gamma irradiation and methylene blue enhances the performance of activated carbon, enabling energy storage solutions that are efficient, cost-effective, and environmentally friendly. This approach supports waste reduction and resource conservation by transforming rice husk waste into high-performance materials, aligning with the goals of cleaner production and sustainable energy technology development. The research emphasizes innovative practices to meet global energy needs sustainably.

1 Introduction

Energy storage devices are becoming increasingly essential in the modern era. Renewable energy sources are being harnessed for power generation in many economies. However, these still need some intermittent and less controllable limitations and often rely on local climate conditions for their feasibility.[1,2] In these cases, energy storage technology meets energy requirements while ensuring sustainability and efficiency.[3–5] Supercapacitors are an example of energy storage technology showing great promise: they can deliver energy quickly and facilitate faster charging times, have elevated specific capacitance and superior power density values, and endure longer life cycles than many batteries.[6] Supercapacitors are categorized into electrical double-layer capacitors (EDLCs) that use an electrostatic charge to produce capacitance and pseudocapacitors that store energy through fast and reversible faradaic redox reactions.[7,8]

Activated carbon is the preferred choice over other carbon materials for manufacturing electrodes for energy storage devices.[9–11] In addition to their relatively low cost, they exhibit high specific surface areas, have tuneable pore distributions, and can be developed from biomass.[12,13] Numerous biomass types are suitable raw materials for synthesizing activated carbon, with rice husk having high potential in Asia driven by its abundant availability as a waste product from the rice milling process.[14] Rice husk disposal can be problematic due to its high silica content.[15] However, this can be advantageous for energy storage applications, providing a mesoporous structure

[a]*Kamnoetvidya Science Academy, 999 Moo 1, Pa Yup Nai, Wangchan, Rayong 21210, Thailand. E-mail: suranan.a@kvis.ac.th*

[b]*Frontier Research Center (FRC), Vidyasirimedhi Institute of Science and Technology, 555 Moo 1, Pa Yup Nai, WangChan, Rayong 21210, Thailand*

[c]*Thailand Institute of Nuclear Technology, Ongkharak, Nakhon Nayok, 26120, Thailand. E-mail: tanagorn@tint.or.th*

† Electronic supplementary information (ESI) available. See DOI: https://doi.org/10.1039/d4su00701h

‡ These authors contributed equally to this work.

to the activated carbon when the silica is removed.[16] This makes rice husk an ideal candidate for supercapacitor development.

Activated carbon is poorly conductive and hydrophobic,[17–20] and therefore, introducing heteroatoms into the carbon framework is a strategy for adding pseudocapacitive effects, which enhance its utility in supercapacitor systems.[3] Recent efforts to improve supercapacitor efficiency have focused on modifying the structure of activated carbons through doping with nitrogen[21] and sulfur.[22] Nitrogen enhances ion transfer capabilities and electronic conductivity, while sulfur induces pseudocapacitive effects, reduces interfacial resistance, and increases hydrophilicity, enhancing charge transfer speed.[8,23–25]

Methylene blue, a popular cationic dye employed in coloring processes, offers a sustainable solution as an adsorbent.[26] In the case of methylene blue, activated carbon can absorb nitrogen and sulfur atoms, resulting in improved energy storage efficiency and wastewater treatment.[27] This is beneficial for improving the supercapacitor's performance and promoting environmental sustainability by resolving the challenge of dye-laden effluents.[28]

Gamma irradiation, along with electron and high-energy photon irradiation, is gaining attention as a technique for modifying the properties of materials.[29] Initially, studies on particle irradiation focused on the treatment and modification of carbon materials, resulting in changes in their mechanical, electronic, and magnetic properties,[30,31] highlighting its promise as a material fabrication tool.[32,33] The optimized gamma irradiation technique can enhance the electrical conductivity,[34] specific surface area,[35] and pore volume of carbons[36] while being environmentally benign, cost-effective, and energy-efficient.[30,37]

This research aims to investigate the impact of methylene blue doping and post-treatment by gamma radiation on rice husk-derived activated carbon (GAC) properties in its use as a supercapacitor material. Another significant benefit of this research is demonstrating the dual functionality of activated carbon for methylene blue removal and its subsequent reuse as a supercapacitor electrode, contributing to the goal of zero waste.

2 Methodology

2.1. Preparation of activated carbon

Glutinous rice husk (GRH) was collected from Surin, Thailand. GRH was thoroughly washed with deionized water to eliminate surface impurities and then dried at 60 °C for 48 hours. After drying, the GRH was finely ground and sieved to achieve a particle size of 74 μm. Subsequently, GRH-derived activated carbon (GAC) was prepared by impregnating GRH with 33 wt% potassium hydroxide (KOH) in a 1 : 2 weight ratio. The mixture was dried at 80 °C for 72 hours before carbonization in a furnace at 800 °C for 2 hours under a nitrogen flow, at a heating rate of 5 °C min^{-1}. The resulting solid was subsequently washed with 0.1 M sulfuric acid (H_2SO_4), followed by distilled water until the pH of the washings was neutral, before drying at 80 °C for 72 hours, as shown in Scheme 1.

2.2. Modification of activated carbon with methylene blue

2.2.1. Doping of unmodified GAC without post-treatment. In a typical batch, 200 mg of GAC was mixed with 400 ml of a 50 ppm aqueous methylene blue solution. The mixture was stirred using an orbital shaker at 150 rpm and maintained at 25 °C for 9 hours. After stirring, the material (GAC-Stir) was filtered and dried at 80 °C for 12 hours.

2.2.2. Doping and post-treatment by hydrothermal processing. GAC (200 mg) was mixed with 400 ml of a 50 ppm aqueous methylene blue solution, and the suspension was then stirred with an orbital shaker at 150 rpm at 25 °C for 9 hours. The solution was then placed into a 500 ml Teflon hydrothermal reactor, and hydrothermal treatment was conducted at 180 °C for 12 hours. The material (GAC-Hdt) was collected and dried at 80 °C for 12 hours.

2.2.3. Doping and post-treatment using gamma irradiation. The GAC was doped following the protocol mentioned above. For the post-treatment, samples were purged with nitrogen for 40 min before being exposed to gamma irradiation from a ^{60}Co source (JS 8900 IR-155, Nordion) at the Thailand Institute of Nuclear Technology, Thanyaburi, Thailand. The irradiation was performed at a dose rate of 8.3 kGy per h, with a total dose of 25 kGy, affording the sample labeled GAC-25. The samples were also subjected to 50 kGy or 100 kGy using the same method and were labeled as GAC-50 and GAC-100, respectively.

2.3. Characterization

2.3.1. Physical and chemical characterization of carbon materials. The morphologies of GAC, GAC-Stir, GAC-Hdt, GAC-25, GAC-50, and GAC-100 were investigated using Scanning Electron Microscopy (SEM, JEOL JSM-7610F), with Energy-Dispersive X-ray (EDX) spectroscopy used for mapping the distribution of elements such as carbon (C), oxygen (O), nitrogen (N), and sulfur (S) within the samples. Surface functional groups were identified using Fourier transform infrared spectroscopy (FTIR, Bruker Tensor 27), performed from 4000 cm^{-1} to 500 cm^{-1}. The elemental composition of the surface was ascertained through X-ray photoelectron spectroscopy (XPS, JPS9010MC spectrometer, JEOL Ltd) using a MgKα radiation source. The degree of graphitization and the presence

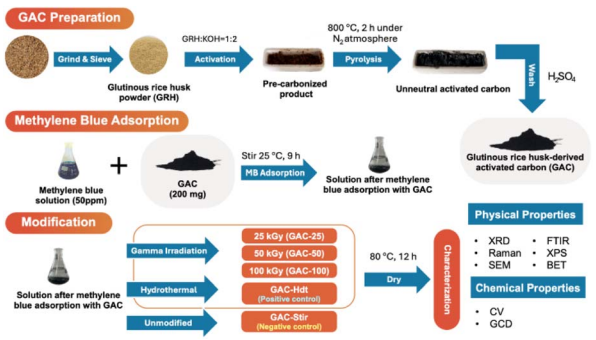

Scheme 1 The preparation of activated carbon and doped activated carbon.

of defects within the sample were assessed using Raman spectroscopy (Raman, XploRA™ PLUS HOLIBA) over the range of 1000 cm^{-1} to 1800 cm^{-1} at an excitation wavelength of 532 nm. The crystallinity of the samples was characterized using powder X-ray diffraction (XRD, Bruker D8 ADVANCE) coupled with CuKα radiation, covering angles (2θ) between 10° and 80°. The specific surface area and pore volumes were characterized using nitrogen adsorption–desorption isotherms (BELSORP-max, Microtrac BEL crop.) following the Brunauer–Emmett–Teller (BET) method. Samples were degassed at 573 K for 5 hours prior to measurement. The pore volume was determined by the amount of nitrogen absorbed at 77 K with a relative pressure ($p/p°$) ratio of approximately 0.999.

2.3.2. Electrochemical measurements. The electrochemical performance of the samples was assessed using a three-electrode configuration. The electrodes were prepared by mixing GAC, GAC-Stir, GAC-Hdt, GAC-25, GAC-50, or GAC-100 with a polytetrafluoroethylene (PTFE) binder and carbon black in a weight ratio of 80 : 10 : 10. The mixture was combined with ethanol to form a homogeneous dough, which was then dried at 80 °C 12 hours. Subsequently, the material was punched with a thickness of 0.090 mm and a diameter of 3 mm and 4 mm to serve as the working electrode and counter electrode, respectively. The samples were rolled into a freestanding electrode.

The electrochemical performance of the prepared electrodes was evaluated using three-electrode Swagelok-type cells with 3 M H_2SO_4 electrolyte, a Hg/Hg_2Cl_2 reference electrode, and a Celgard 2400 film as a separator. Cyclic voltammetry (CV) measurements were conducted at scan rates of 5, 10, 20, 50, and 100 mV s^{-1} over a potential range of −0.05 to 0.65 V. Galvanostatic charge/discharge (GCD) tests were performed at current densities ranging from 0.5 to 5.0 A g^{-1}. A stability test was also carried out using the GCD method at a current density of 2.0 A g^{-1} for 3000 cycles. For the three-electrode test, the specific capacitance of samples was calculated using the following equation: $C_{sp} = \frac{I_m \Delta t}{\Delta V}$, where C_{sp} is the specific capacitance (F g^{-1}), I_m is the current density (A g^{-1}), Δt is the time interval during discharge time (s), and ΔV is the potential window (V).

3 Results and discussion

3.1. Material characterization

The product yield of GAC is approximately 12.5%. The morphologies of GAC samples are shown in Fig. 1. Each material exhibits an interconnected porous structure, with the pore formation characteristics of KOH activation. The decomposition of KOH releases carbon monoxide (CO) and carbon dioxide (CO_2), as shown in the equation below. These gases disrupt the carbon structure, thus creating the observed porosity.[38,39]

$$6KOH + 2C \rightarrow 2K + 3H_2 + 2K_2CO_3 \quad (1)$$

$$KOH + C \rightarrow K + CO + 1/2H_2 \quad (2)$$

$$K_2CO_3 \rightarrow K_2O + CO_2 \quad (3)$$

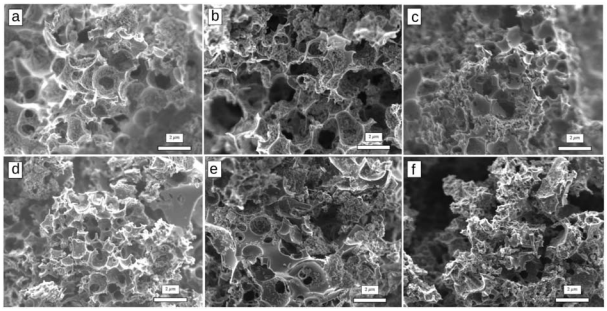

Fig. 1 The SEM images of (a) GAC, (b) GAC-Stir, (c) GAC-Hdt, (d) GAC-25, (e) GAC-50, and (f) GAC-100.

The morphology of the activated carbon framework does not change significantly after the adsorption of methylene blue, as the amount of methylene blue relative to activated carbon is small, with 200 mg of activated carbon in 400 ml of a 50 ppm aqueous methylene blue solution. However, gamma irradiation results in some degradation of the carbon framework, with higher doses (50 and 100 kGy) causing the formation of voids. These voids alter the structural integrity of the material, which leads to poor electron transportation. In contrast, hydrothermal treatment (Fig. 1(c), GAC-Hdt) does not appear to result in degradation, with the image revealing many interconnected tiny pores. SEM-EDX images for GACs are provided in the Appendix (Fig. S1–S6).†

The textural properties of GACs were characterized using nitrogen adsorption–desorption isotherms, as shown in Fig. 2. According to the IUPAC classification,[37] all GACs exhibit type I and type IV isotherms. Type I isotherms are consistent with micropores in the sample,[40] while type IV isotherms typically occur in mesoporous materials[41] with H4-type hysteresis at high relative pressure. BET analysis was performed to compare the surface areas, pore volumes, and porosities of the GAC materials (Table 1). The blocking of pores by methylene blue results in a slight decline of S_{BET} in GAC-Stir relative to GAC. The significant enhancement in the S_{BET} of GAC-Hdt compared to GAC is due to extensive micropores formed during hydrothermal operations.

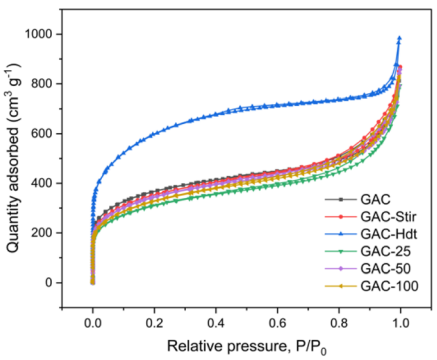

Fig. 2 Nitrogen adsorption–desorption isotherms for GACs.

Table 1 Specific surface areas and pore volumes for GAC materials

Sample	S_{BET} ($m^2\ g^{-1}$)	V_{total} (cm^3)	V_{micro} (cm^3)	Average pore size (nm)
GAC (no MB)	1218	1.17	0.49	3.83
GAC-Stir	1208	1.16	0.46	3.85
GAC-25	1003	1.11	0.30	4.45
GAC-50	1200	1.16	0.33	3.87
GAC-100	1147	1.18	0.30	4.15
GAC-Hdt	1847	1.37	1.01	2.98

Regarding gamma irradiation, the GAC-25 and GAC-100 samples display a slight reduction in the surface area relative to GAC-Stir, with GAC-50 achieving the highest surface area among the irradiated samples. Micropores of gamma-irradiated samples have been destroyed, resulting in a decrease in S_{BET}. Additionally, the trend can be attributed to the effect of irradiation on the pore structure. Specifically, a 25 kGy dose likely provides insufficient energy to significantly modify morphologies, while a 100 kGy dose may cause excessive morphological changes and a reduced surface area. The 50 kGy dose, however, appears to optimize the porosity enhancement, resulting in the highest BET surface area and favorable ion transport pathways.[42] In terms of porous structures, GAC-Stir, GAC-25, GAC-50, and GAC-100 have mesopore volumes of 0.70, 0.81, 0.83, and 0.88 $cm^3\ g^{-1}$, respectively, suggesting that as the dose of gamma irradiation increases, the overall pore structure shifts towards larger mesopores with respect to GAC-Stir. This transition is beneficial for ion diffusion during electrochemical processes, as mesopores facilitate the efficient transport of electrolyte ions.[43] GAC-Hdt, on the other hand, has the highest micropore volume of 1.01 cm^3 with a total volume of 1.37 cm^3. These findings suggest that hydrothermal treatment is more effective in increasing micropore volume and enhancing the charge storage ability,[44] while gamma irradiation transforms micropores into mesopores, improving the rate of ion transport.

The X-ray diffraction profiles of GACs are presented in Fig. 3(a). All samples are amorphous[45,46] and exhibit broad diffraction peaks at 2θ around 24° and 42°, attributed to the (002) and (100) reflections in graphitic carbon, respectively. There is no shift in either diffraction peak after doping with methylene blue, suggesting that the overall structural arrangement is preserved.[47]

The Raman spectra of GAC samples are shown in Fig. 3(b), and in all cases, the D band and G band are located at 1340 cm^{-1} and 1570 cm^{-1}, respectively. The D band corresponds to the A_{1g} vibration and is associated with defects and heteroatoms within the carbon lattice. In contrast, the G band represents the E_{2g} mode symmetry and signifies the presence of a sp^2 carbon framework resulting from the stretching vibrations of C–C bonds in graphitic planes and aromatic rings.[46–48] The I_D/I_G ratio values reflect the level of disorder or defects within the structure. GAC-Stir decreases in I_D/I_G to 1.07, confirming a more graphitic nature than GAC.[49] In the case of the hydrothermal technique, the I_D/I_G of GAC-Hdt is significantly higher (I_D/I_G, 1.39), similar to that of gamma-irradiated GAC-25 (I_D/I_G, 1.23). However, at higher doses of gamma irradiation (50 kGy and 100 kGy), the I_D/I_G values were lower, 0.99 for GAC-50 and 0.86 for GAC-100, respectively. This is consistent with research by Vatankhah *et al.*, who reported that gamma irradiation could reduce the degree of graphitization and induce significant disorder as shown by higher I_D/I_G values, but elevated dosages might also lead to decreases in I_D/I_G.[50]

Fourier-transform infrared (FT-IR) spectra were obtained for all GAC samples to highlight the functional groups present (Fig. 4). The broad absorption band at 3400 cm^{-1} is attributed to O–H/N–H stretching vibrations.[51,52] The peak at 1600 cm^{-1} corresponds to C=O stretching and C=C stretching, while the prominent peak at 1070 cm^{-1} is attributed to the stretching vibrations of C–O–R bonds.[49] Additionally, GAC-Stir and GAC-25 exhibit 1320 cm^{-1} and 1380 cm^{-1} peaks consistent with C–O stretching and N–CH_3 stretching vibrations, respectively.[45,53] However, these bands are not observed in the spectra of GAC-Hdt, indicating that hydrothermal pretreatment may result in the loss of some functionality groups, in contrast to gamma irradiation. The loss of surface functional groups may be disadvantageous, decreasing the wettability of activated carbon with aqueous electrolytes.

XPS analysis was conducted to examine the surface chemistry of doped activated carbon with or without post-treatment, with the results highlighted in Fig. 5. While the presence of four main peaks in Fig. 5(a), C 1s (284.7 eV), N 1s (400 eV), O 1s (532 eV), and S 2p (163.7 eV), confirm the successful incorporation of methylene blue within the carbon matrix *via* adsorption, hydrothermal, and gamma irradiation, it is crucial to focus on the element nitrogen, which significantly contributes to pseudocapacitive effects, as sulfur is present only in relatively small

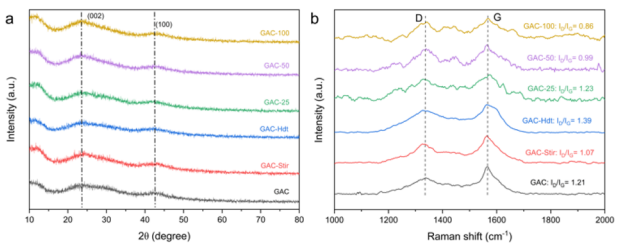

Fig. 3 (a) XRD patterns and (b) Raman spectra of GAC materials.

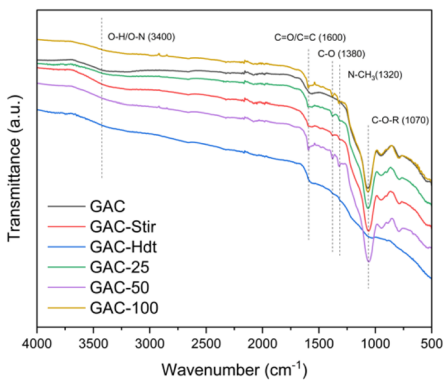

Fig. 4 FT-IR spectra of GACs over the range of 500–4000 cm^{-1}.

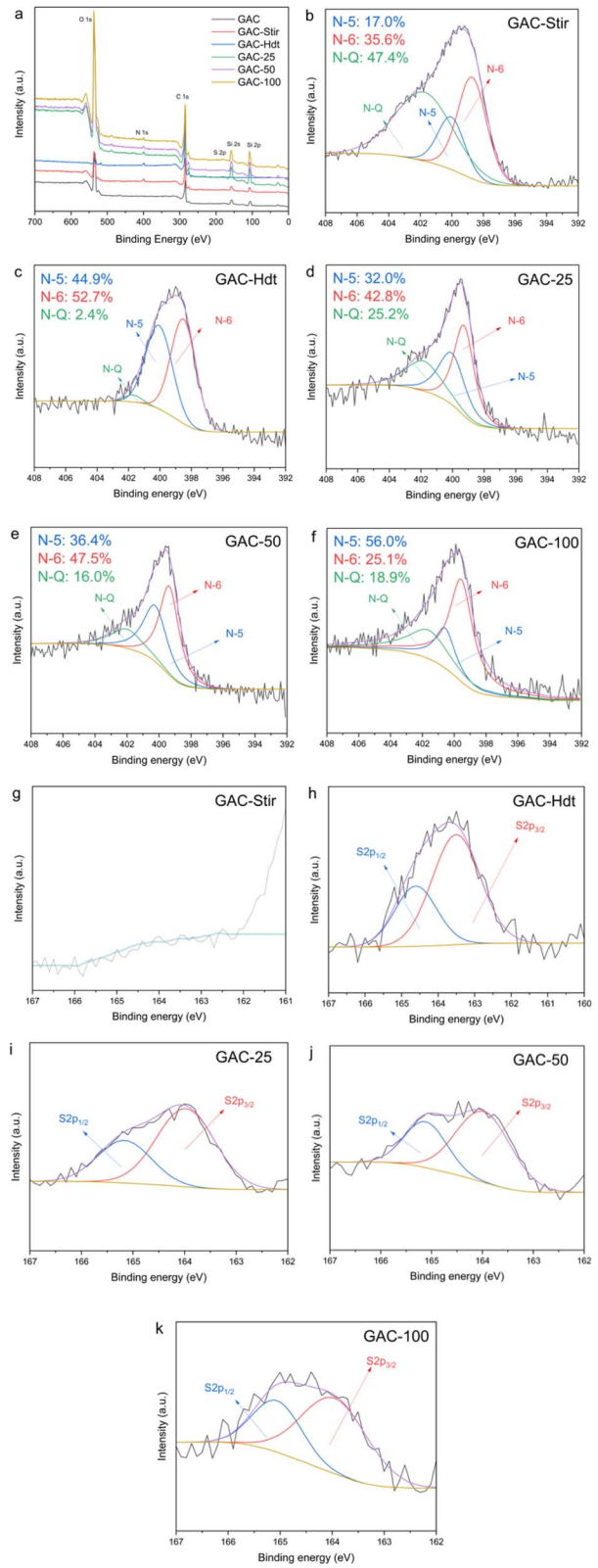

Fig. 5 (a) XPS survey scan spectra of GACs: the N 1s high-resolution XPS scan of (b) GAC-Stir; (c) GAC-Hdt; (d) GAC-25; (e) GAC-50; and (f) GAC-100, and the S 2p high-resolution XPS scan of (g) GAC-Stir; (h) GAC-Hdt; (i) GAC-25; (j) GAC-50; and (k) GAC-100.

amounts. The nitrogen and sulfur dopants came from methylene blue. During doping, methylene blue could degrade and release nitrogen and sulfur atoms as inorganic ions ready to incorporate into the activated carbon. Therefore, the N 1s peaks were deconvoluted (Fig. 5(b)–(f)) into N-6 (pyridinic-N), N-5 (pyrrolic-N), and N-Q (quaternary-N) at 399.1 eV, 400.8 eV, and 401.9 eV, respectively.[54,55] GAC-Stir comprised 17.0% N-5, 35.6% N-6, and 47.4% N-Q. After post-treatment, the content of N-Q significantly decreased to 2.4% in GAC-Hdt and 25.2% in GAC-25. Meanwhile, N-5 and N-6 dramatically increased to 44.9% and 52.7% in GAC-Hdt, respectively. GAC-25 also had a higher percentage of N-5 and N-6, 32.0% and 42.8%, respectively. GAC-50 showed a balanced distribution of nitrogen species, with 36.4% N-5, 47.5% N-6, and 16.0% N-Q. GAC-100 had the highest N-5 content of 56.0%, with 25.1% N-6 and a relatively lower N-Q content of 18.9%. N-5 and N-6 are beneficial for improving capacitance due to their involvement in faradaic reactions occurring at the electrode–electrolyte interface, specifically at the surface sites where redox reactions occur, enhancing pseudocapacitance. In contrast, N-Q mainly contributes to conductivity but provides less pseudocapacitance.[4,56] The reduction of N-Q and the increase of N-5 and N-6 after post-treatment, especially in GAC-Hdt and GAC-100, indicate that post-treatment enhances the electrode's pseudocapacitive behavior, which is expected to improve the overall electrochemical performance of the supercapacitor. These results indicate the changes in the active site of activated carbon for methylene blue from N-Q to N-5 and N-6 that are attributed to pseudocapacitive effects after post-treatment, such as hydrothermal and gamma irradiation.

The electrochemical performance of the samples was evaluated using a three-electrode test system with 3 M H_2SO_4 as the electrolyte. As shown in Fig. 6(a), the CV curves of GACs measured at a scan rate of 5 mV s^{-1} display a quasi-rectangular shape, which is characteristic of the electrochemical behavior of a typical electrical double-layer capacitor (EDLC) in supercapacitors. Furthermore, redox peaks were observed around 0.2 V/0.27 V at the electrode/electrolyte interface.[55] The reversible redox reaction of methylene blue is responsible for the modification of activated carbon,[57,58] which gives credence to its incorporation in enhancing electrochemical performance. The electrochemical properties of samples were assessed through kinetic calculations using eqn (1s)† and were analyzed for charge storage mechanisms, indicating diffusion or surface capacitance control. The results in Fig. 8s(a)† confirm that GAC-Stir, GAC-Hdt, GAC-25, GAC-50, and GAC-100 exhibit hybrid charge storage devices, displaying pseudocapacitive features. The capacitance contribution rate was calculated (eqn (2s)†) at a scan rate of 5 mV s^{-1}, as shown in Fig. 8s(b).† GAC-Stir, GAC-Hdt, GAC-25, GAC-50, and GAC-100 mechanisms comprise approximately equal capacitive and diffusion components.

Fig. 6(b) displays the GCD curves of GACs at a current density of 0.5 A g^{-1}. The GCD curve of GACs exhibits a quasi-triangular shape. The specific capacitance was calculated from the slope of the discharge. As a result, GAC, GAC-Stir, GAC-Hdt, GAC-25, GAC-50, and GAC-100 exhibited specific capacitances of 69.2 F g^{-1}, 85.0 F g^{-1}, 242.1 F g^{-1}, 127.9 F g^{-1}, 124.3 F g^{-1}, and 104.2 F

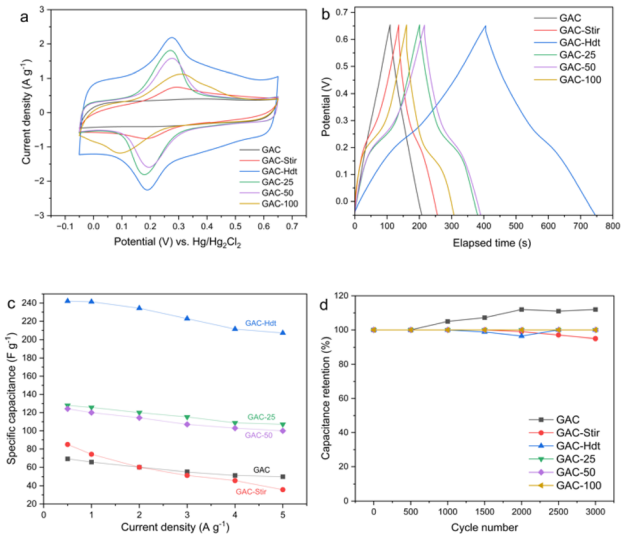

Fig. 6 Electrochemical performance performed in a three-electrode system: (a) CV curves at a scan rate of 5 mV s^{-1}; (b) GCD curves at a current density of 0.5 A g^{-1}; (c) specific capacitance at various current densities; (d) capacitance retention for 3000 cycles of GACs.

g^{-1} at 0.5 A g^{-1}, respectively. The specific capacitance of GAC-Stir (85.0 F g^{-1}) indicates a 22.8% increase compared to that of the untreated GAC (69.2 F g^{-1}). Further treatments, such as hydrothermal or gamma irradiation at the optimal dosage (25 kGy), significantly enhanced the specific capacitance by 249.9% and 84.8%, respectively. The massive increase in the specific capacitance of GAC-Hdt can be attributed to its much greater specific surface area (Table 1). Although GAC-25 has a smaller surface area compared to GAC-Stir, it provides higher specific capacitance, which suggests that the contribution of N-5 and N-6 in GAC-25 may contribute additional specific capacitance through pseudocapacitive effects, as observed by the more dominant peak in the CV profile compared to GAC-Stir.

Although GAC-50 and GAC-100 exhibited relatively high specific capacitances of 124.3 F g^{-1} and 104.2 F g^{-1}, respectively, they did not have higher specific capacitance than GAC-25. While GAC-50 and GAC-100 have larger surface areas and higher amounts of nitrogen functional groups (N-5 and N-6), which typically enhance pseudocapacitive effects, the superior performance of GAC-25 can be attributed to the appropriate presence of N-Q groups. These quaternary nitrogen groups (N-Q) are known to increase the material's conductivity, improving charge transfer efficiency.[4,56] The enhanced conductivity provided by N-Q in GAC-25 may compensate for the lower surface area and N-5 and N-6 contents. This is also supported by the more pronounced peaks in the CV profiles of GAC-25 compared to GAC-50 and GAC-100, indicating better electrochemical performance.

As the current density increases from 0.5 A g^{-1} to 5.0 A g^{-1} in Fig. 6(c), the retention of the capacities of GAC, GAC-Stir, GAC-Hdt, GAC-25, and GAC-50 was 72.3%, 42%, 85.5%, 83.8%, and 80.5%, respectively. The cycling stability of GAC, GAC-Stir, GAC-Hdt, GAC-25, and GAC-50 for 3000 cycles, performed at 2 A g^{-1}, is demonstrated in Fig. 6(d). The specific capacitance retention of GAC increased to 112%, likely due to the full wetting of the electrode material. This complete wetting allows for continuous electrolyte diffusion inside the open-porous channels of the activated carbon, thereby enhancing the activation of the materials.[24] While the specific capacitance retention of GAC-Stir dropped to 95%, GAC-Hdt and all gamma-irradiated activated carbons exhibited excellent stability, with 100% capacitance retention despite pseudocapacitive effects. These results demonstrate the capability of retaining supercapacitors' performance through reversible redox action from pseudocapacitive effects. Further images of CV graphs with different scan rates and current densities are provided in the Appendix (Fig. S7).†

4 Conclusion

Glutinous rice husks were used to synthesize activated carbon (GAC) as the basis of supercapacitor electrodes. Methylene blue, which contains heteroatoms, was integrated into the carbon framework, in addition to post-treatment using gamma irradiation or hydrothermal processing to modify the surface chemistry of the activated carbon. Among samples subjected to gamma irradiation (25–100 kGy), the 25 kGy sample (GAC-25) exhibited the highest specific capacitance of 127.9 F g^{-1} at 0.5 A g^{-1} in 3 M H_2SO_4 aqueous electrolyte, even though it has a lower specific surface area than materials not subjected to post-treatment (GAC and GAC-Stir). GAC-50 and GAC-100 also did not outperform GAC-25. This is likely due to enhanced appropriate reactive surface chemistry and conductivity.

On the other hand, hydrothermally treated GAC-Hdt achieved a specific capacitance of 242.1 F g^{-1} due to its relatively high specific surface area. The capacitance retention of all samples after post-treatment is 100% after 3000 charges and discharge cycles at a current density of 2.0 A g^{-1}. Despite the highest specific capacitance exhibited by GAC-Hdt, gamma-irradiated samples still showed pseudocapacitive effects at a high scan rate in the CV profile, which is absent in GAC-Hdt. This suggests that gamma irradiation can serve as post-treatment in carbon materials doped with methylene blue, without the need for corrosive chemicals or heat.

Data availability

The data supporting this article have been included as part of the ESI.†

Author contributions

Conceptualization: T. S., and S. A.; formal analysis: T. A., N. S., J. S., N. C., S. I., T. S., and S. A.; investigation: T. A., N. S., J. S., N. C., S. I., T. S., and S. A.; resources: T. S. and S. A.; writing—original draft: T. A., N. S., and J. S.; writing—review & editing: T. A., N. S, J. S., T. S., and S. A.; visualization: T. S.; supervision: T. S. and S. A.; funding acquisition: T. S. and S. A. All authors have read and agreed to the published version of the manuscript.

Conflicts of interest

There are no conflicts to declare.

Acknowledgements

The authors are indebted to the support provided by (i) the Thailand Institute of Nuclear Technology (Public Organization) and the Thailand Science Research and Innovation (TSRI) and (iii) the National Science, Research and Innovation Fund (NSRF). Furthermore, the authors would like to acknowledge the guidance and mentorship provided by the Centre of Excellence for Energy Storage Technology (CEST), the School of Energy Science and Engineering (ESE), the Frontier Research Center (FRC), the Vidyasirimedhi Institute of Science and Technology (VISTEC), and Kamnoetvidya Science Academy (KVIS). We also would like to thank Assoc. Prof. Dr Christopher B. Smith for kind suggestions and language checking.

References

1 C. S. Yang, Y. S. Jang and H. K. Jeong, Bamboo-based activated carbon for supercapacitor applications, *Curr. Appl. Phys.*, 2014, **14**(12), 1616–1620.
2 H. Ibrahim, A. Ilinca and J. Perron, Energy storage systems-Characteristics and comparisons, *Renewable Sustainable Energy Rev.*, 2008, **12**, 1221–1250.
3 D. Wu, T. Wang, L. Wang and D. Jia, Hydrothermal synthesis of nitrogen, sulfur co-doped graphene and its high performance in supercapacitor and oxygen reduction reaction, *Microporous Mesoporous Mater.*, 2019, **290**, 109556.
4 A. Gopalakrishnan and S. Badhulika, Effect of self-doped heteroatoms on the performance of biomass-derived carbon for supercapacitor applications, *J. Power Sources*, 2020, **480**, 228830.
5 S. Anand, M. Wasi Ahmad, A. Syed, A. H. Bahkali, M. Verma, B. Hye Kim, *et al.*, Walnut shell derived N, S co-doped activated carbon for solid-state symmetry supercapacitor device, *J. Ind. Eng. Chem.*, 2024, **129**, 309–320.
6 E. Y. L. Teo, L. Muniandy, E. P. Ng, F. Adam, A. R. Mohamed, R. Jose, *et al.*, High surface area activated carbon from rice husk as a high performance supercapacitor electrode, *Electrochim. Acta*, 2016, **192**, 110–119.
7 G. P. Pandey, A. C. Rastogi and C. R. Westgate, All-solid-state supercapacitors with poly(3,4-ethylenedioxythiophene)-coated carbon fiber paper electrodes and ionic liquid gel polymer electrolyte, *J. Power Sources*, 2014, **245**, 857–865.
8 J. Jiang, L. Zhang, X. Wang, N. Holm, K. Rajagopalan, F. Chen, *et al.*, Highly ordered macroporous woody biochar with ultra-high carbon content as supercapacitor electrodes, *Electrochim. Acta*, 2013, **113**, 481–489.
9 J. Rivera-Utrilla, M. Sánchez-Polo, V. Gómez-Serrano, P. M. Álvarez, M. C. M. Alvim-Ferraz and J. M. Dias, Activated carbon modifications to enhance its water treatment applications. An overview, *J. Hazard. Mater.*, 2011, **187**, 1–23.
10 J. D. Atkinson, Z. Zhang, Z. Yan and M. J. Rood, Evolution and impact of acidic oxygen functional groups on activated carbon fiber cloth during NO oxidation, *Carbon N Y*, 2013, **54**, 444–453.
11 S. Yaglikci, Y. Gokce, E. Yagmur and Z. Aktas, The performance of sulphur doped activated carbon supercapacitors prepared from waste tea, *Environ. Technol.*, 2020, **41**(1), 36–48.
12 C. A. M. Moraes, I. J. Fernandes, D. Calheiro, A. G. Kieling, F. A. Brehm and M. R. Rigon, *et al.*, Review of the rice production cycle: by-products and the main applications focusing on rice husk combustion and ash recycling, *Waste Management and Research*. SAGE Publications Ltd; 2014. Vol. 32. pp. 1034–48.
13 J. Chen, J. Liu, D. Wu, X. Bai, Y. Lin, T. Wu, *et al.*, Improving the supercapacitor performance of activated carbon materials derived from pretreated rice husk, *J. Energy Storage*, 2021, **15**, 44.
14 M. Yeleuov, C. Seidl, T. Temirgaliyeva, A. Taurbekov, N. Prikhodko, B. Lesbayev, *et al.*, Modified activated graphene-based carbon electrodes from rice husk for supercapacitor applications, *Energies*, 2020, **13**(18), 4943.
15 S. Wang, K. Zou, Y. Qian, Y. Deng, L. Zhang and G. Chen, Insight to the synergistic effect of N-doping level and pore structure on improving the electrochemical performance of sulfur/N-doped porous carbon cathode for Li-S batteries, *Carbon N Y*, 2019, **144**, 745–755.
16 S. Zhang, X. Shi, R. Wróbel, X. Chen and E. Mijowska, Low-cost nitrogen-doped activated carbon prepared by polyethylenimine (PEI) with a convenient method for supercapacitor application, *Electrochim. Acta*, 2019, **294**, 183–191.
17 K. Zou, Y. Deng, J. Chen, Y. Qian, Y. Yang, Y. Li, *et al.*, Hierarchically porous nitrogen-doped carbon derived from the activation of agriculture waste by potassium hydroxide and urea for high-performance supercapacitors, *J. Power Sources*, 2018, **378**, 579–588.
18 K. Charoensook, C. L. Huang, H. C. Tai, V. V. K. Lanjapalli, L. M. Chiang, S. Hosseini, *et al.*, Preparation of porous nitrogen-doped activated carbon derived from rice straw for high-performance supercapacitor application, *J. Taiwan Inst. Chem. Eng*, 2021, **120**, 246–256.
19 S. Uppugalla, R. Pothu, R. Boddula, M. A. Desai and N. Al-Qahtani, Nitrogen and sulfur co-doped activated carbon nanosheets for high-performance coin cell supercapacitor device with outstanding cycle stability, *Emergent Mater.*, 2023, **6**(4), 1167–1176.
20 Y. Huang, S. L. Candelaria, Y. Li, Z. Li, J. Tian, L. Zhang, *et al.*, Sulfurized activated carbon for high energy density supercapacitors, *J. Power Sources*, 2014, **252**, 90–97.
21 B. Li, F. Dai, Q. Xiao, L. Yang, J. Shen, C. Zhang, *et al.*, Nitrogen-doped activated carbon for a high energy hybrid supercapacitor, *Energy Environ. Sci.*, 2016, **9**(1), 102–106.
22 D. Zhang, M. Han, B. Wang, Y. Li, L. Lei, K. Wang, *et al.*, Superior supercapacitors based on nitrogen and sulfur co-doped hierarchical porous carbon: Excellent rate capability and cycle stability, *J. Power Sources*, 2017, **358**, 112–120.

23 M. Kotal, H. Kim, S. Roy and I. K. Oh, Sulfur and nitrogen co-doped holey graphene aerogel for structurally resilient solid-state supercapacitors under high compressions, *J. Mater. Chem. A*, 2017, **5**(33), 17253–17266.

24 H. Gul, A. Shah, H. A. ul and S. Bilal, Achieving ultrahigh cycling stability and extended potential window for supercapacitors through asymmetric combination of conductive polymer nanocomposite and activated carbon, *Polymers*, 2019, **11**(10), 1678.

25 K. J. L. dos Santos, G. E. de S. dos Santos, S. á Í. M. G. L. de, A. H. Ide, J. L. da S. Duarte, S. H. V. de Carvalho, *et al.*, Wodyetia bifurcata biochar for methylene blue removal from aqueous matrix, *Bioresour. Technol.*, 2019, **293**, 122093.

26 W. Tong, F. Huang, L. Chen, H. Wu and X. Zhou, Methylene blue enhanced bamboo activated carbon as high performance supercapacitor electrode materials, *Ind. Crops Prod.*, 2022, **180**, 114786.

27 E. Adhamash, R. Pathak, Q. Qiao, Y. Zhou and R. McTaggart, Gamma-radiated biochar carbon for improved supercapacitor performance, *RSC Adv.*, 2020, **10**(50), 29910–29917.

28 A. R. Vatankhah, M. A. Hosseini and S. Malekie, The characterization of gamma-irradiated carbon-nanostructured materials carried out using a multi-analytical approach including Raman spectroscopy, *Appl. Surf. Sci.*, 2019, **488**, 671–680.

29 E. Samiei, S. Mohammadi and M. Torkzadeh-Mahani, Effect of gamma-irradiation on electrochemical properties of ZnCo2O4-rGO for supercapacitor application, *Diamond Relat. Mater.*, 2022, **127**, 109157.

30 N. S. Mohd Nor, M. Deraman, R. Omar, F. R. Awitdrus, N. H. Basri, *et al.*, Influence of gamma irradiation exposure on the performance of supercapacitor electrodes made from oil palm empty fruit bunches, *Energy*, 2015, **79**(C), 183–194.

31 E. M. Abou Hussein and N. A. El-Alaily, Study on the Effect of Gamma Radiation on Some Spectroscopic and Electrical Properties of Lithium Borate Glasses, *J. Inorg. Organomet. Polym. Mater.*, 2018, **28**(3), 1214–1225.

32 R. Qindeel, Effect of gamma radiation on morphological & optical properties of ZnO nanopowder, *Results Phys.*, 2017, **7**, 807–809.

33 B. Mast, I. Gerardy, Y. Pontikes, W. Schroeyers, B. Reniers, P. Samyn, *et al.*, The effect of gamma radiation on the mechanical and microstructural properties of Fe-rich inorganic polymers, *J. Nucl. Mater.*, 2019, **521**, 126–136.

34 Z. Xu, L. Chen, B. Zhou, Y. Li, B. Li, J. Niu, *et al.*, Nano-structure and property transformations of carbon systems under γ-ray irradiation: a review, *RSC Adv.*, 2013, **3**, 10579–10597.

35 A. Funke and F. Ziegler, Hydrothermal carbonization of biomass: A summary and discussion of chemical mechanisms for process engineering, *Biofuels, Bioprod. Biorefin.*, 2010, **4**, 160–177.

36 T. T. T. Ho, A. Nadeem and K. Choe. A Review of Upscaling Hydrothermal Carbonization, *Energies*. Multidisciplinary Digital Publishing Institute (MDPI); 2024. vol. 17.

37 C. Keluo, T. Zhang and C. Xiaohui, Model construction of micro-pores in shale: a case study of Silurian Longmaxi Formation shale in Dianqianbei area, SW China, *Pet. Explor. Dev.*, 2018, **45**, 412–421.

38 R. Guo, C. Lv, W. Xu, J. Sun, Y. Zhu, X. Yang, *et al.*, Effect of Intrinsic Defects of Carbon Materials on the Sodium Storage Performance, *Adv. Energy Mater.*, 2020, **10**(9), 1903652.

39 O. Oginni, K. Singh, G. Oporto, B. Dawson-Andoh, L. McDonald and E. Sabolsky, Influence of one-step and two-step KOH activation on activated carbon characteristics, *Bioresour. Technol. Rep.*, 2019, **7**, 100266.

40 D. Liu, W. Zhang, H. Lin, Y. Li, H. Lu and Y. Wang, Hierarchical porous carbon based on the self-templating structure of rice husk for high-performance supercapacitors, *RSC Adv.*, 2015, **5**(25), 19294–19300.

41 H. Chen, F. Wang, S. Tong, S. Guo and X. Pan, Porous carbon with tailored pore size for electric double layer capacitors application, *Appl. Surf. Sci.*, 2012, **258**(16), 6097–6102.

42 A. Annisa, I. Prasetyo, D. Swantomo and T. Ariyanto. Surface modification of nanoporous carbon using gamma irradiation treatment as supercapacitor material. In: *AIP Conference Proceedings*, American Institute of Physics Inc.; 2021.

43 Y. Lu, S. Zhang, J. Yin, C. Bai, J. Zhang, Y. Li, *et al.*, Mesoporous activated carbon materials with ultrahigh mesopore volume and effective specific surface area for high performance supercapacitors, *Carbon N Y*, 2017, **124**, 64–71.

44 L. Niu, C. Shen, L. Yan, J. Zhang, Y. Lin, Y. Gong, *et al.*, Waste bones derived nitrogen–doped carbon with high micropore ratio towards supercapacitor applications, *J. Colloid Interface Sci.*, 2019, **547**, 92–101.

45 T. Liu, E. Liu, R. Ding, Z. Luo, T. Hu and Z. Li, Preparation and supercapacitive performance of clew-like porous nanocarbons derived from sucrose by catalytic graphitization, *Electrochim. Acta*, 2015, **173**, 50–58.

46 D. Dong, Y. Zhang, Y. Xiao, T. Wang, J. Wang, C. E. Romero, *et al.*, High performance aqueous supercapacitor based on nitrogen-doped coal-based activated carbon electrode materials, *J. Colloid Interface Sci.*, 2020, **580**, 77–87.

47 X. Zhu, S. Yu, K. Xu, Y. Zhang, L. Zhang, G. Lou, *et al.*, Sustainable activated carbons from dead ginkgo leaves for supercapacitor electrode active materials, *Chem. Eng. Sci.*, 2018, **181**, 36–45.

48 W. Yin, D. Dong, Y. Zhang, T. Wang, J. Wang, C. E. Romero, *et al.*, Effect of annealing temperature on the continuity and conductivity of coal-based carbon films prepared by ball milling, *Appl. Surf. Sci.*, 2020, **30**, 510.

49 M. Xu, D. Li, Y. Yan, T. Guo, H. Pang and H. Xue, Porous high specific surface area-activated carbon with co-doping N, S and P for high-performance supercapacitors, *RSC Adv.*, 2017, **7**(69), 43780–43788.

50 A. R. Vatankhah, M. A. Hosseini and S. Malekie, The characterization of gamma-irradiated carbon-nanostructured materials carried out using a multi-analytical approach including Raman spectroscopy, *Appl. Surf. Sci.*, 2019, **488**, 671–680.

51 Y. Matsumoto and K. Honma, NH stretching vibrations of pyrrole clusters studied by infrared cavity ringdown spectroscopy, *J. Chem. Phys.*, 2007, **127**(18), 184310.
52 S. Sathyamoorthi, N. Phattharasupakun and M. Sawangphruk, Environmentally benign non-fluoro deep eutectic solvent and free-standing rice husk-derived bio-carbon based high-temperature supercapacitors, *Electrochim. Acta*, 2018, **286**, 148–157.
53 A. Misra, P. K. Tyagi, M. K. Singh and D. S. Misra, FTIR studies of nitrogen doped carbon nanotubes, *Diamond Relat. Mater.*, 2006, **15**(2–3), 385–388.
54 N. Chen, Y. Zhou, S. Cao, R. Wang and W. Jiao, A novel strategy for loading metal cocatalysts onto hollow nano-TiO_2 inner surface with highly enhanced H_2 production activity, *Green Energy Environ.*, 2023, **8**(2), 509–518.
55 M. Graś, Ł. Kolanowski, J. Wojciechowski and G. Lota, Electrochemical supercapacitor with thiourea-based aqueous electrolyte, *Electrochem. Commun.*, 2018, **97**, 32–36.
56 S. Ghosh, S. Barg, S. M. Jeong and K. Ostrikov. Heteroatom-Doped and Oxygen-Functionalized Nanocarbons for High-Performance Supercapacitors, *Advanced Energy Materials*. Wiley-VCH Verlag; 2020. vol. 10.
57 H. Chen, F. Yu, G. Wang, L. Chen, B. Dai and S. Peng, Nitrogen and Sulfur Self-Doped Activated Carbon Directly Derived from Elm Flower for High-Performance Supercapacitors, *ACS Omega*, 2018, **3**(4), 4724–4732.
58 Y. Zhang, T. Cai, J. Huang, W. Xing and Z. Yan, Functionalized activated carbon prepared form petroleum coke with high-rate supercapacitive performance, *J. Mater. Res.*, 2016, **31**(23), 3723–3730.